Supplementary Table 1

Figure, Supplementary Figure, and Table Associations.

Figure	Supplementary Figure	Table
1	1, 2, 3	-
2	4, 5, 6	-
3	8	Supp 2
4	9, 10, 11	-
5	12, 13	-
6	14	-
7	15, 16, 17	-
8	18	Supp 3, Supp 4
9	19	1, 2

Supplementary Figure 1

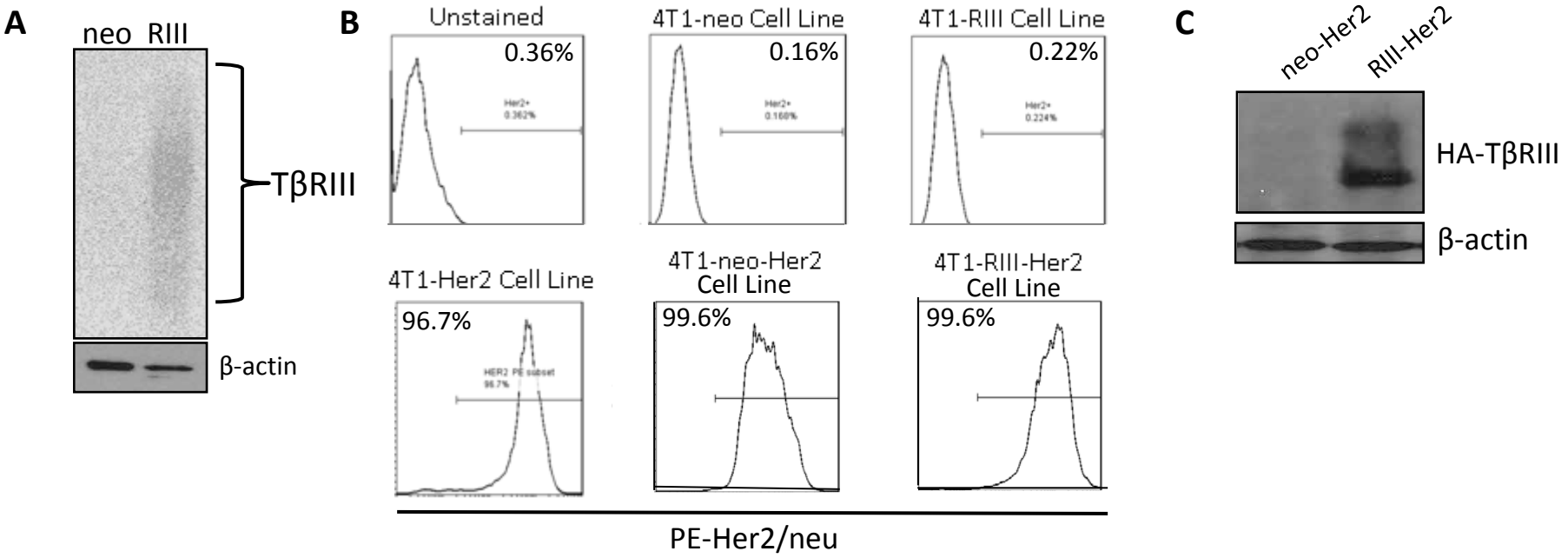

Supplementary Figure 1. 4T1-neo and 4T1-RIII Tumor Cell Lines. (A) ^{125}I-TGF-β binding and crosslinking analysis of the 4T1-neo and 4T1-RIII tumor cell lines. **(B)** Flow cytometry analysis of Her2/neu expression by the 4T1-neo-Her2 and 4T1-RIII-Her2 tumor cell lines. **(C)** anti-hemaglutinin (HA) western blot study of the 4T1-neo-Her2 and 4T1-RIII-Her2 cell lines. All data is mean ± s.e.m. **P* < 0.05. *P* values based on two-tailed student's *t* tests.

Supplementary Figure 2

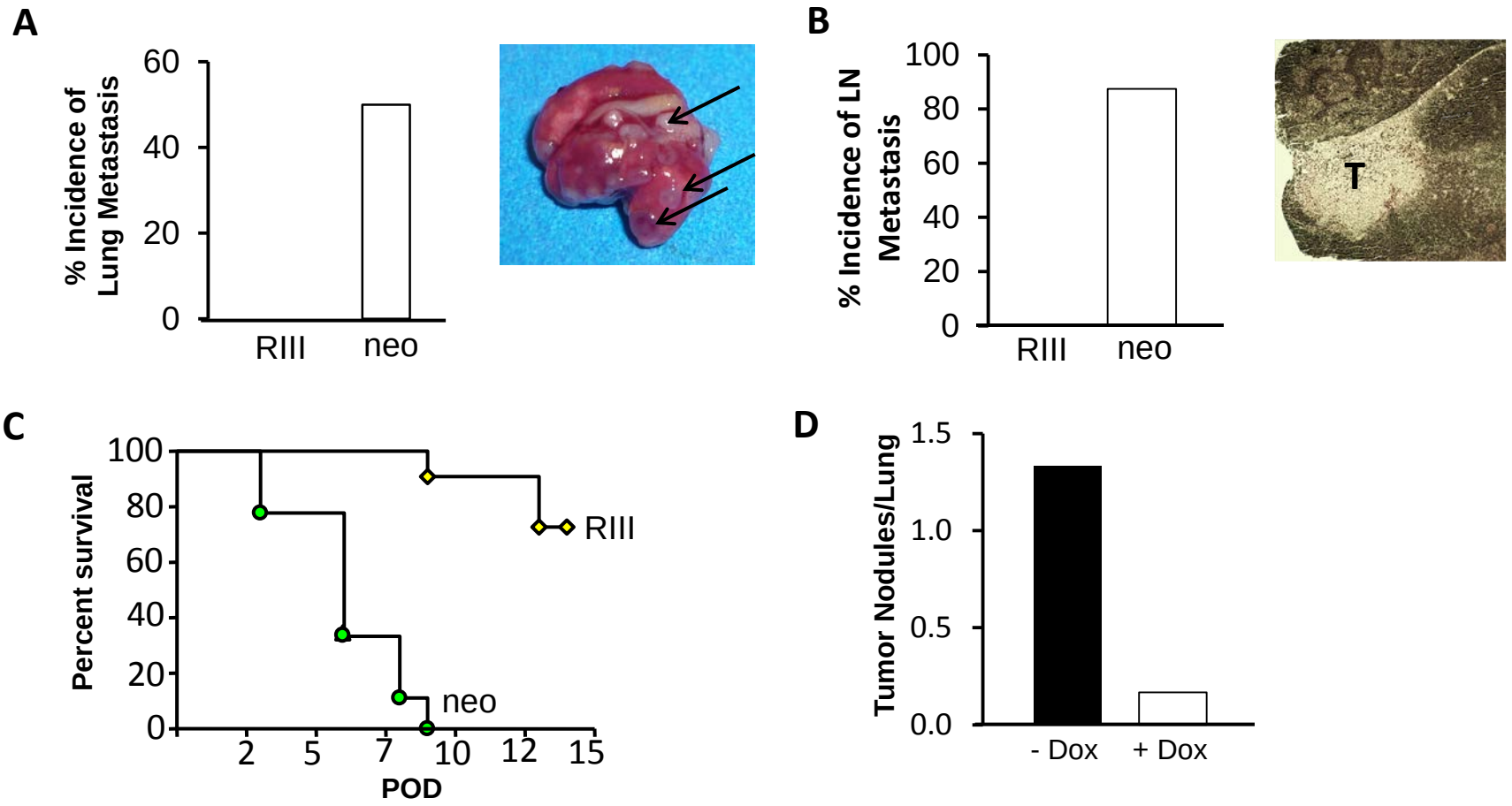

Supplementary Figure 2. TβRIII Expression Suppresses 4T1 Metastatic Progression. **(A)** 4T1 metastatic lung lesions were identified visually during necropsy studies in 4T1-neo and 4T1-RIII tumor-bearing wild type BALB/c mice. **(B)** 4T1 lymph node metastasis was quantified by H&E IHC following the resection of ipsilateral axillary lymph nodes from 4T1-neo and 4T1-RIII tumor-bearing wild type BALB/c mice. T, tumor nodule. **(C)** Percent survival of 4T1-neo and 4T1-RIII tumor-bearing mice following primary tumor resection. POD, post-operative day. **(D)** 4T1-sRIII$_{tet}$ lung metastases quantified by H&E IHC surveillance of resected lung tissue. Dox, doxycycline.

Supplementary Figure 3

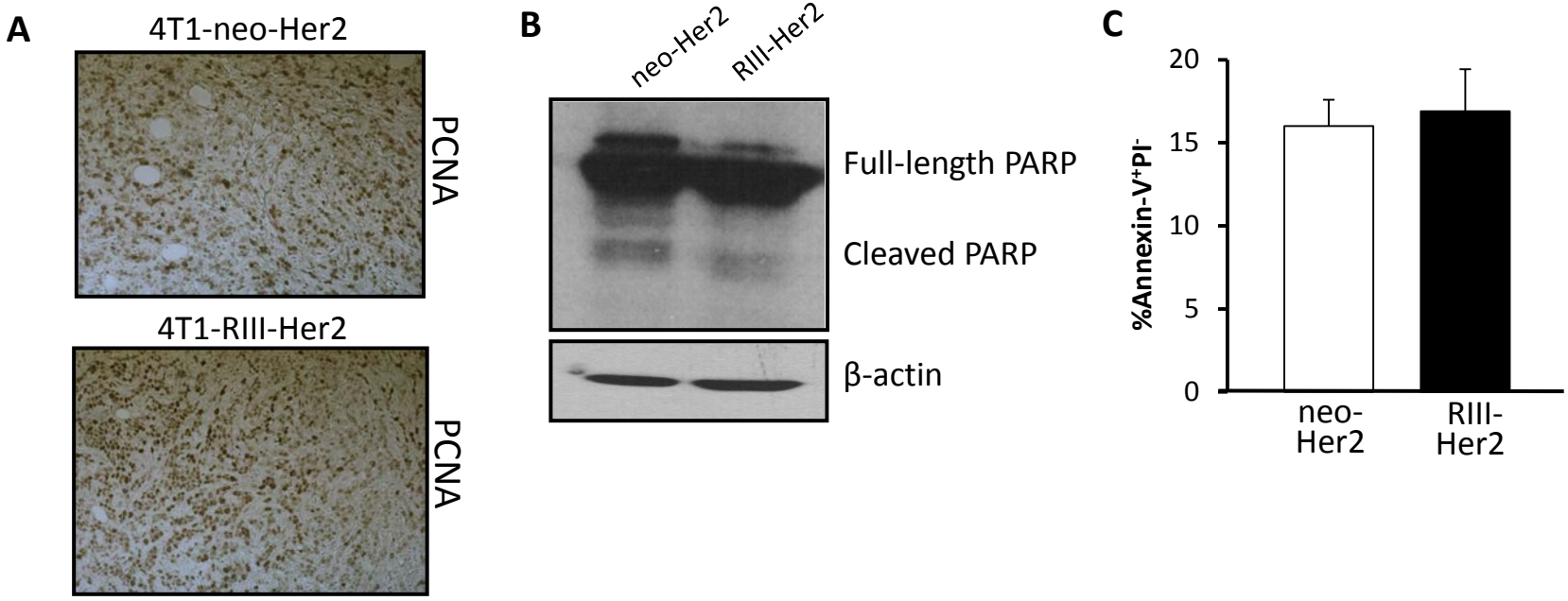

Supplementary Figure 3. TβRIII-Her2/neu Cross-Talk Does Not Affect Tumor Cell Proliferation *In vivo* or Tumor Cell Apoptosis *In vitro*. (A) Proliferating cell nuclear antigen (PCNA) staining of resected 4T1-neo-Her2 and 4T1-RIII-Her2 tumor tissues. 3 tumors per group. **(B)** Anti-poly(ADP-ribose) polymerase (PARP) western blot analysis of the 4T1-neo-Her2 and 4T1-RIII-Her2 tumor cell lines. Representative of 3 independent experiments. **(C)** Annexin-V/PI flow cytometry analysis of the 4T1-neo-Her2 and 4T1-RIII-Her2 cell lines. Representative of two independent experiments.

Supplementary Figure 4

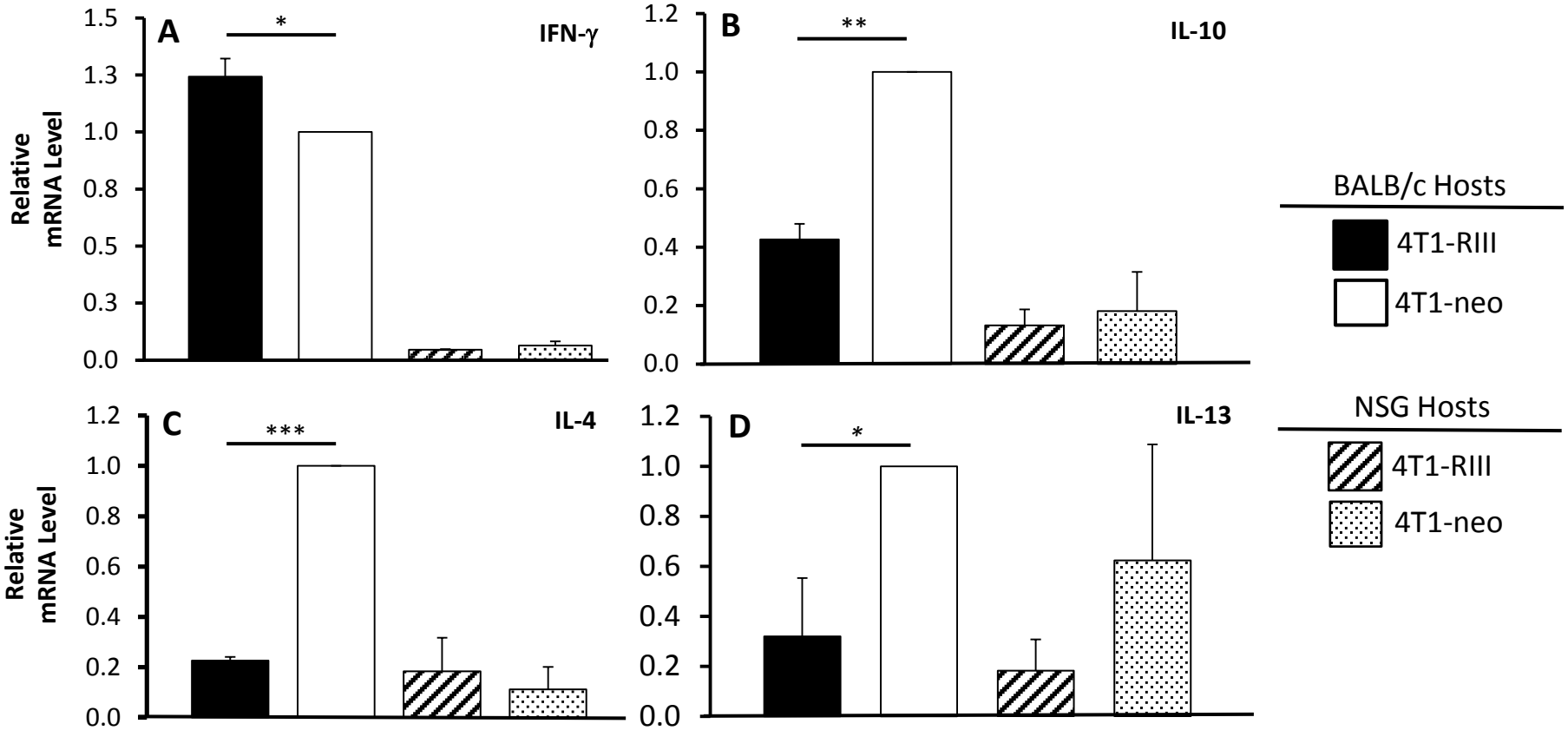

Supplementary Figure 4. Loss of TβRIII Promotes T_H2 Polarization in the Tumor Microenvironment. qRT-PCR analysis of cytokine gene expression in resected 4T1-neo and 4T1-RIII tumors. 5 tumors per group, representative of 3 independent experiments. All data is mean ± s.e.m. **P* < 0.05, ***P* < 0.005, ****P* < 0.0005. *P* values based on two-tailed student's *t* test.

Supplementary Figure 5

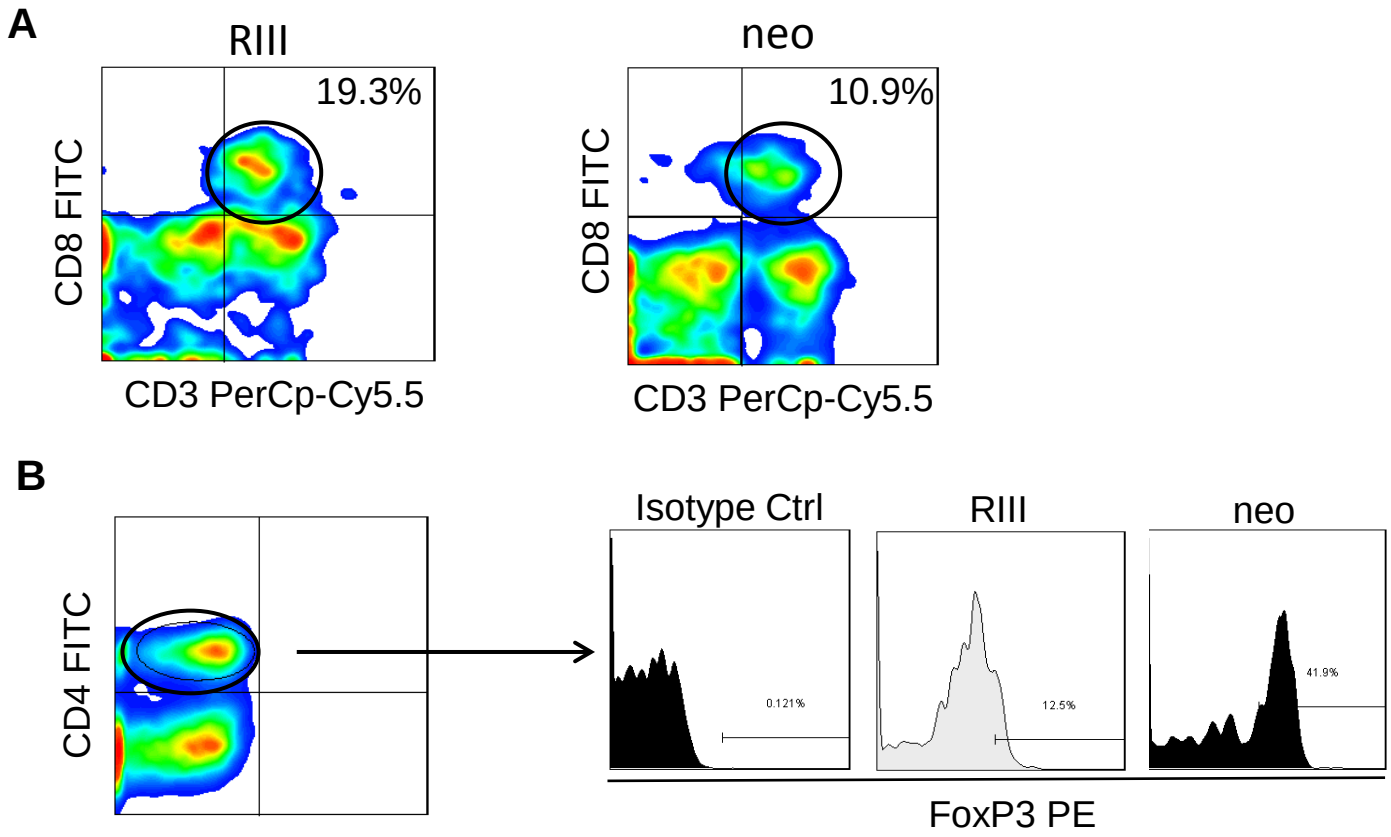

Supplementary Figure 5. Flow Cytometry Analysis of Tumor-draining Lymph Node (TDLN) Tissues Resected from 4T1-neo or 4T1-RIII Tumor-bearing Mice. (A) Representative data from $CD3^+CD8^+$ T cell flow analysis. Percentages based on viable TDLN cells. **(B)** Representative data from $CD4^+FoxP3^+$ T cell flow analysis. Percent $FoxP3^+$ cells quantitated based on the viable TDLN $CD4^+$ T cell population.

Supplementary Figure 6

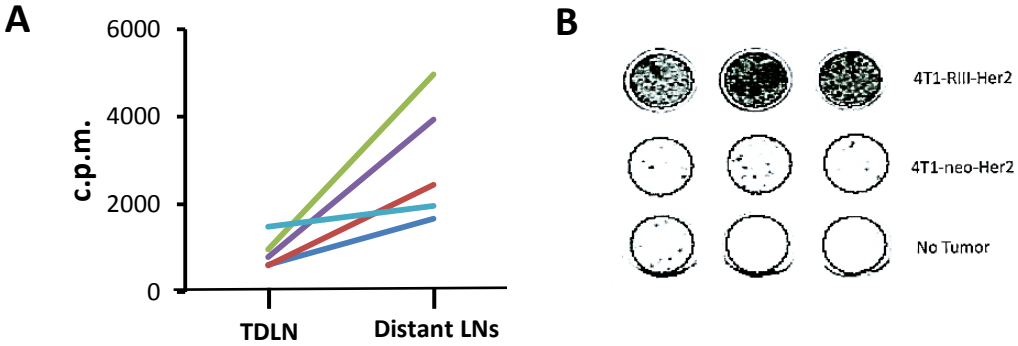

Supplementary Figure 6. Supportive T cell Response Data. **(A)** T cell proliferation capacity of tumor-draining lymph node antigen presenting cells is suppressed relative to distant LN tissues. Each line represents a single mouse; c.p.m., counts per minute. **(B)** Her2-specific IFN-γ ELISPOT analysis. Representative wells.

Supplementary Figure 7

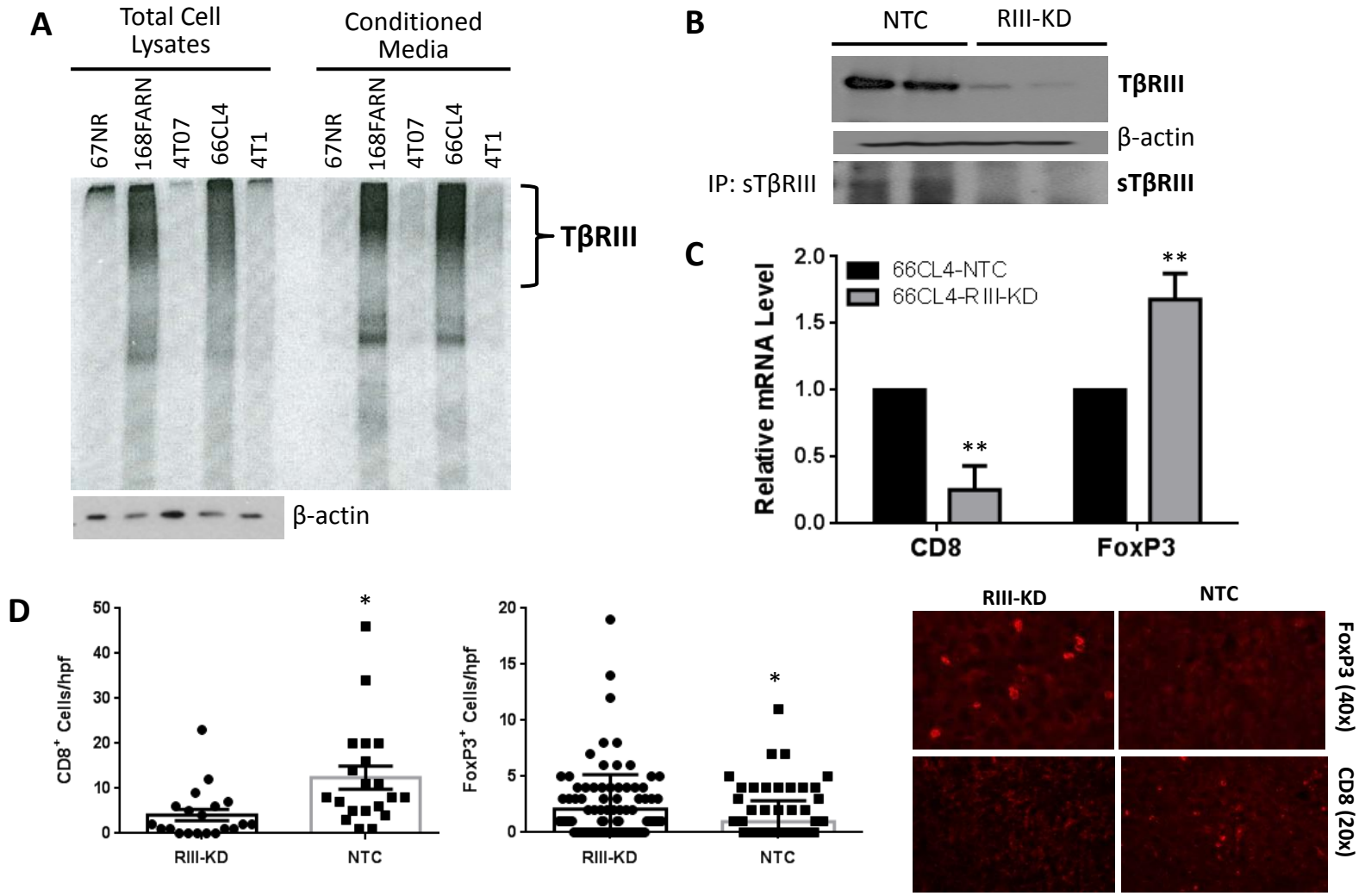

Supplementary Figure 7. Suppressing TβRIII Expression in the 66CL4 Murine Mammary Carcinoma Cell Line. (A) ^{125}I-TGF-β binding and crosslinking analysis of murine mammary carcinoma cell lines. Conditioned media samples reflect shed sTβRIII. **(B)** Western blot analysis confirming TβRIII and sTβRIII silencing in the 66CL4-RIII-KD cell lines relative to 66CL4-NTC control cell lines by lentiviral transduction. KD, knockdown. NTC, non-targeted shRNA control. IP, immunoprecipitation prior to Western blot. **(C)** qrt-PCR analysis of CD8 and FoxP3 gene expression by both 66CL4-NTC and 66CL4-RIII-KD tumors. 5 tumors per group, representative of 2 independent experiments. *P* value < 0.001 based on two-way ANOVA. **(D)** CD8 and FoxP3 IHC of 66CL4-NTC and 66CL4-RIII-KD Tumors. 10-20 40x fields per tumor for FoxP3, 10-20 20x fields per tumor for CD8, 2-5 tumors per group. Representative images shown on right. *P* value < 0.001 based on Mann-Whitney U test. All data is mean ± s.e.m.

Supplementary Table 2

TβRIII Expression by Normal Skin Tissue, Benign Nevi, and Primary Melanomas.

Log2 median-centered ratio	TβRIII		
	Normal	Benign Nevus	Primary Melanoma
max	1.10	1.44	1.53
90th	1.10	1.44	0.65
75th	1.10	1.16	0.36
median	0.77	0.74	-0.49
25th	0.75	0.34	-0.84
10th	0.75	-0.09	-1.15
min	0.75	-0.09	-1.57

Data derived from the Haqq dataset, Oncomine 4.4.

Supplementary Figure 8

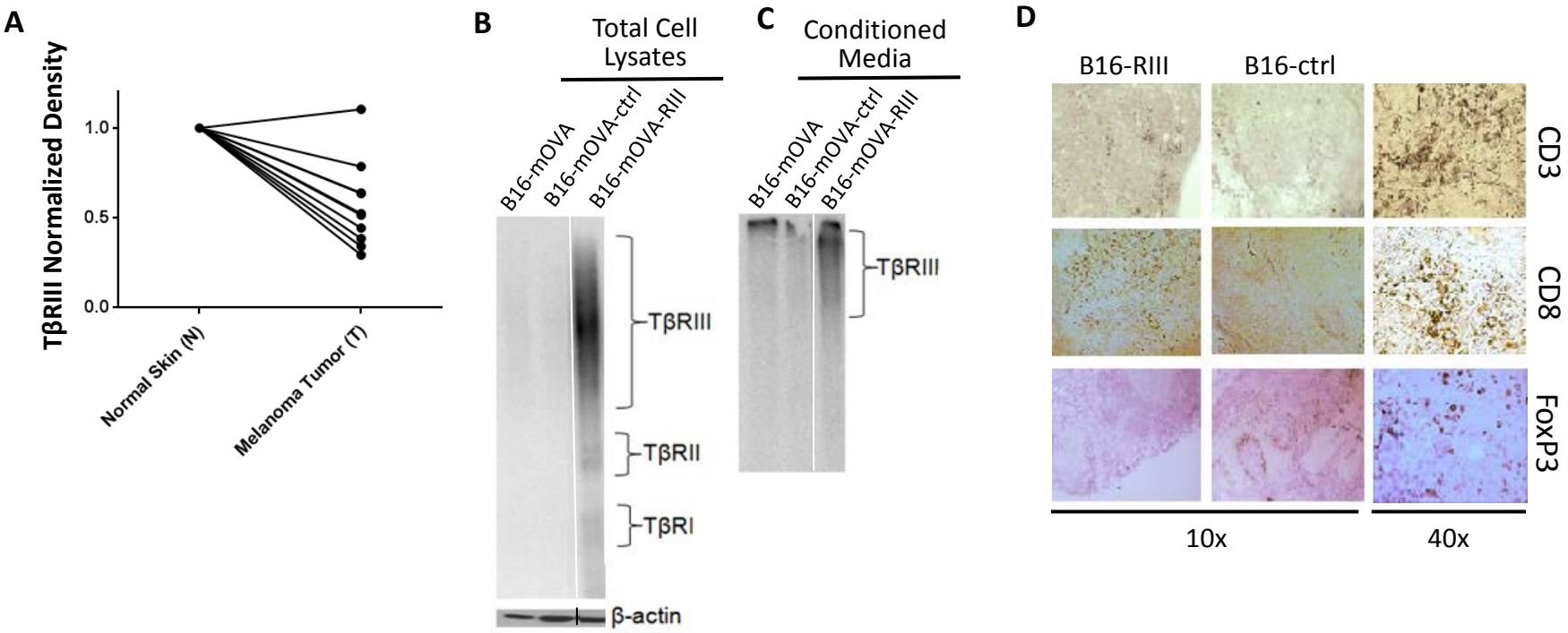

Supplementary Figure 8. Human Melanoma TβRIII Expression and TβRIII-expressing B16 Melanoma Cell Lines. (A) Density analysis of human melanoma tissue TβRIII DNA hybridization blot. All data normalized to paired normal skin tissue sample. Density analysis performed using Image J software. *P* = 0.0039, Wilcoxan matched-pairs signed rank test. **(B)** ^{125}I-TGF-β binding and crosslinking analysis of B16-mOVA-RIII and B16-mOVA-ctrl stable cell line total cell lysates. **(C)** ^{125}I-TGF-β binding and crosslinking study of conditioned media harvested from the B16-mOVA-RIII and B16-mOVA-ctrl stable cell lines. **(D)** CD3, CD8, and FoxP3 IHC performed on resected B16-mOVA-ctrl and B16-mOVA-RIII tumors. 10x (left) and 40x (right) representative fields shown. 3 tumors analyzed per group.

Supplementary Figure 9

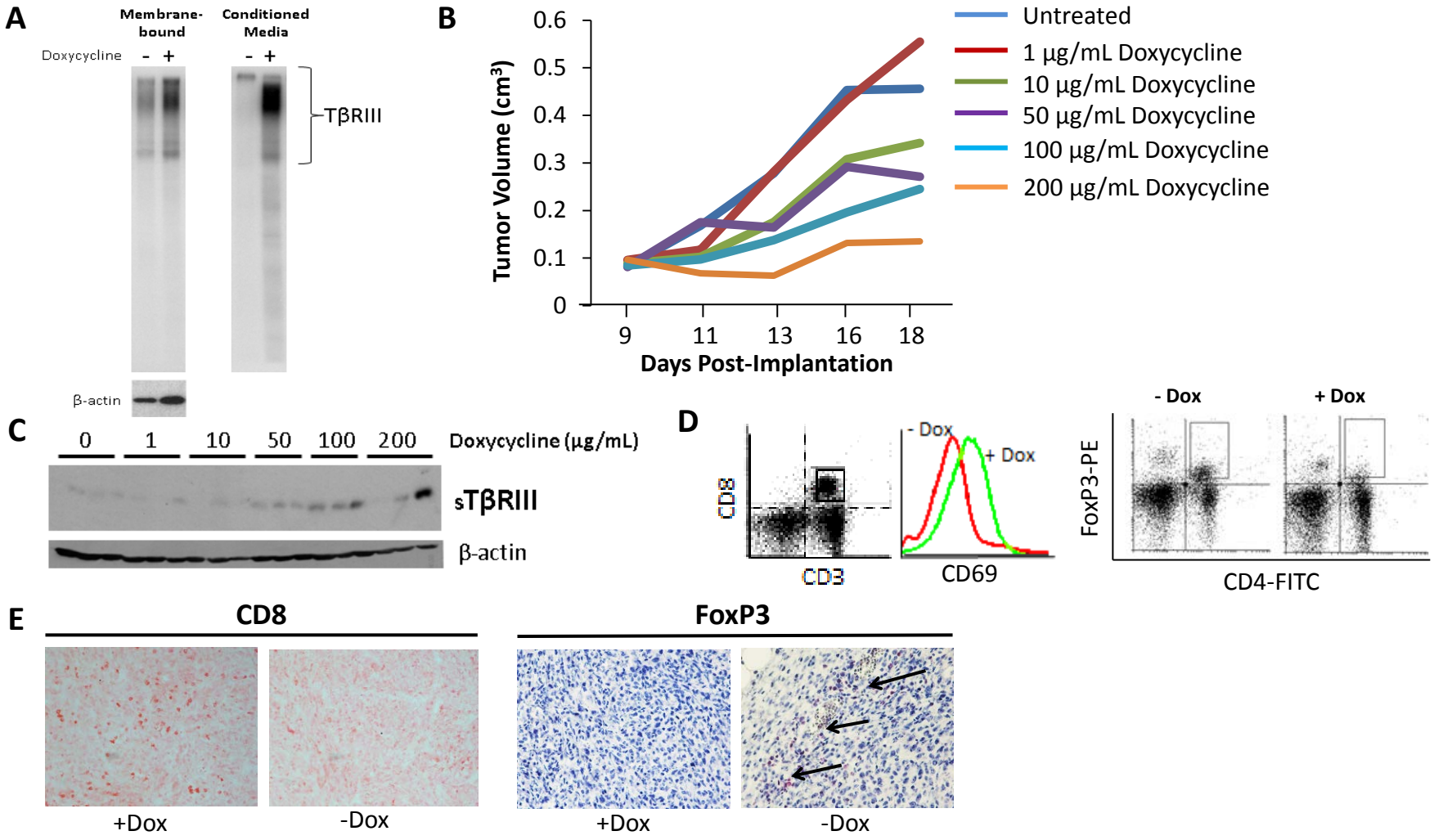

Supplementary Figure 9. Generation of a Tet-on sTβRIII-expressing 4T1 Tumor Line (4T1-sRIIItet). (A) ^{125}I-TGF-β binding and crosslinking analysis of total cell lysates and conditioned media derived from a stable tet-inducible sTβRIII-expressing 4T1 tumor cell line in the presence and absence of doxycycline. **(B)** *In vivo* doxycycline titration following 4T1-sRIIItet tumor implantation. Doxycycline delivered via the water supply. **(C)** Whole tissue western blot screening of *in situ* sTβRIII expression in resected 4T1-sRIIItet tumor tissues at increasing doxycycline concentrations. **(D)** Representative flow cytometry analysis of $CD3^+CD8^+CD69^+$ and $CD4^+FoxP3^+$ T cell analysis in TDLNs resected from 4T1-$sRIII_{tet}$ tumor-bearing mice in the presence or absence of doxycycline (Dox). **(E)** CD8 and FoxP3 4T1 tumor IHC in the presence or absence of Dox. CD8, no counterstain. Representative of 5 examined tumors.

Supplementary Figure 10

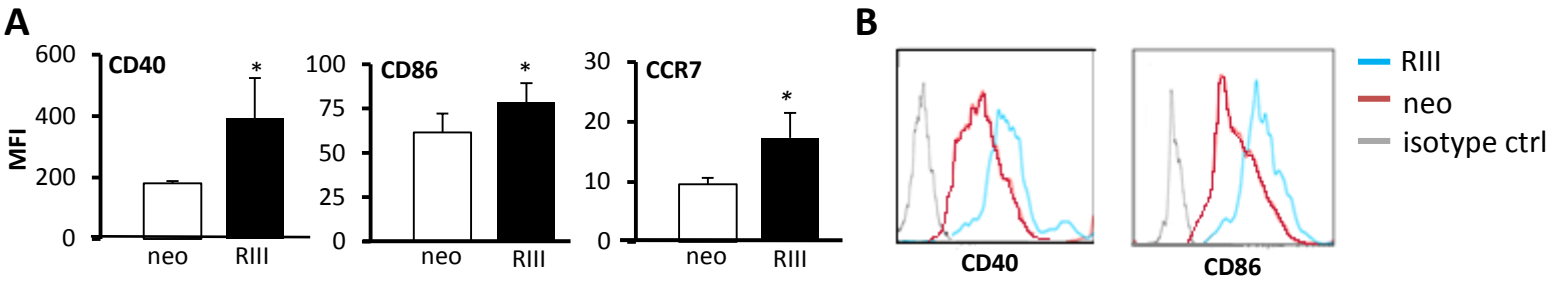

Supplementary Figure 10. DCs Isolated from the TDLNs of 4T1-RIII Tumor-bearing Mice Exhibit a Mature Phenotype. Flow cytometry of $CD11c^+$ DC populations in TDLNs. 8 mice per experiment. Data pooled from 2 independent experiments. *Right*, representative flow histograms of CD40 and CD86 surface expression. All data is mean ± s.e.m. $*P < 0.05$. All *P* values based on two-tailed student's *t* tests.

Supplementary Figure 11

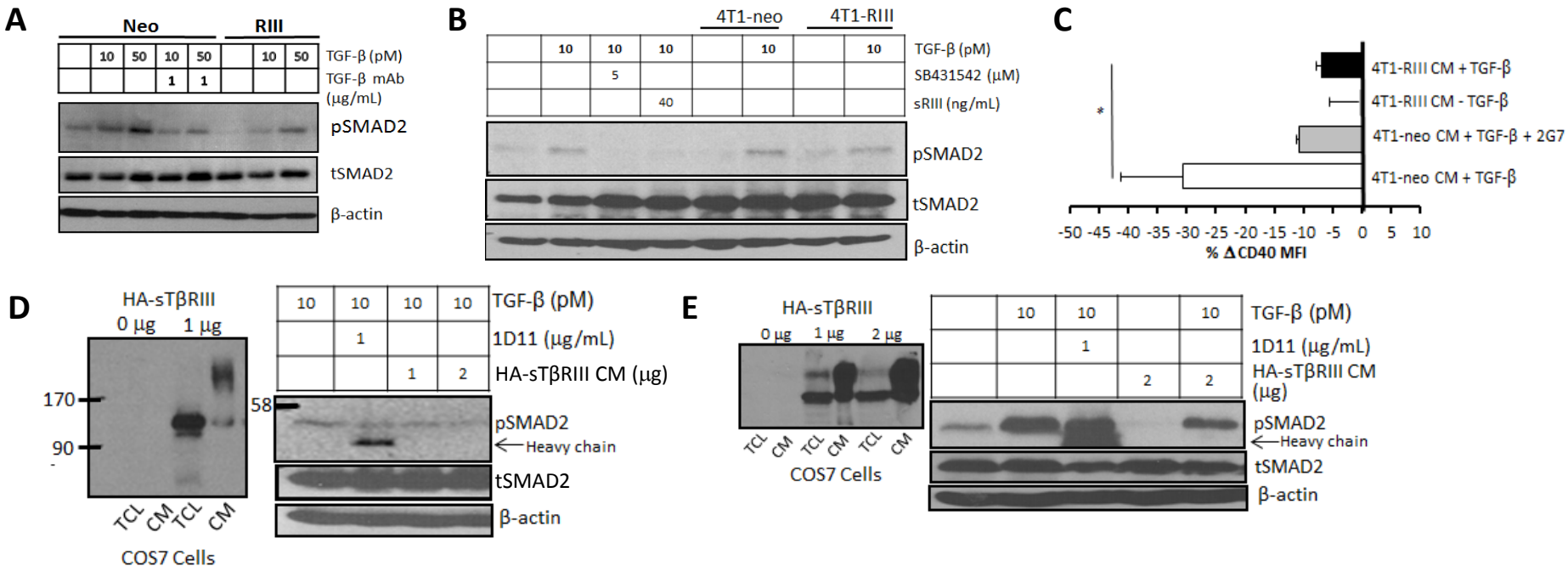

Supplementary Figure 11. Tumor-expressed sTβRIII Inhibits TGF-β-dependent Signaling in DCs. **(A)** pSmad2 Western blot of a TGF-β-treated splenic DC line in the presence of either 4T1-neo or 4T1-RIII CM. pSmad2, phosphorylated Smad2. tSMAD2, total Smad2. CM, conditioned media. **(B)** pSmad2 Western blot of TGF-β-treated bone marrow-derived DCs in the presence and absence of 4T1-neo and 4T1-RIII CM. SB431542, a type I TGF-β receptor serine/threonine kinase inhibitor; sRIII, recombinant soluble TβRIII. **(A)** and **(B)** representative of 3 independent experiments. **(C)** Flow cytometry of DC CD40 expression in the presence and absence of 4T1-RIII CM. Data pooled from 3 independent experiments. 2G7, pan-anti-TGF-β mAb. MFI, mean fluorescence intensity. **(D)** pSmad2 western blot analysis of a TGF-β-treated splenic DC line in the presence and absence of sTβRIII-CM. *left*, anti-HA western blot analysis of total cell lysates (TCLs) and CM of sTβRIII-transfected COS7 cells. 1D11, pan-TGF-β monoclonal antibody. **(E)** pSmad2 western blot of TGF-β-treated BMDCs in the presence and absence of sTβRIII-CM. *left*, anti-HA western blot analysis of TCLs and CM of sTβRIII-transfected COS7 cells. **(D)** and **(E)** representative of 2 independent experiments; heavy chain refers to 1D11 immunoglobulin.

Supplementary Figure 12

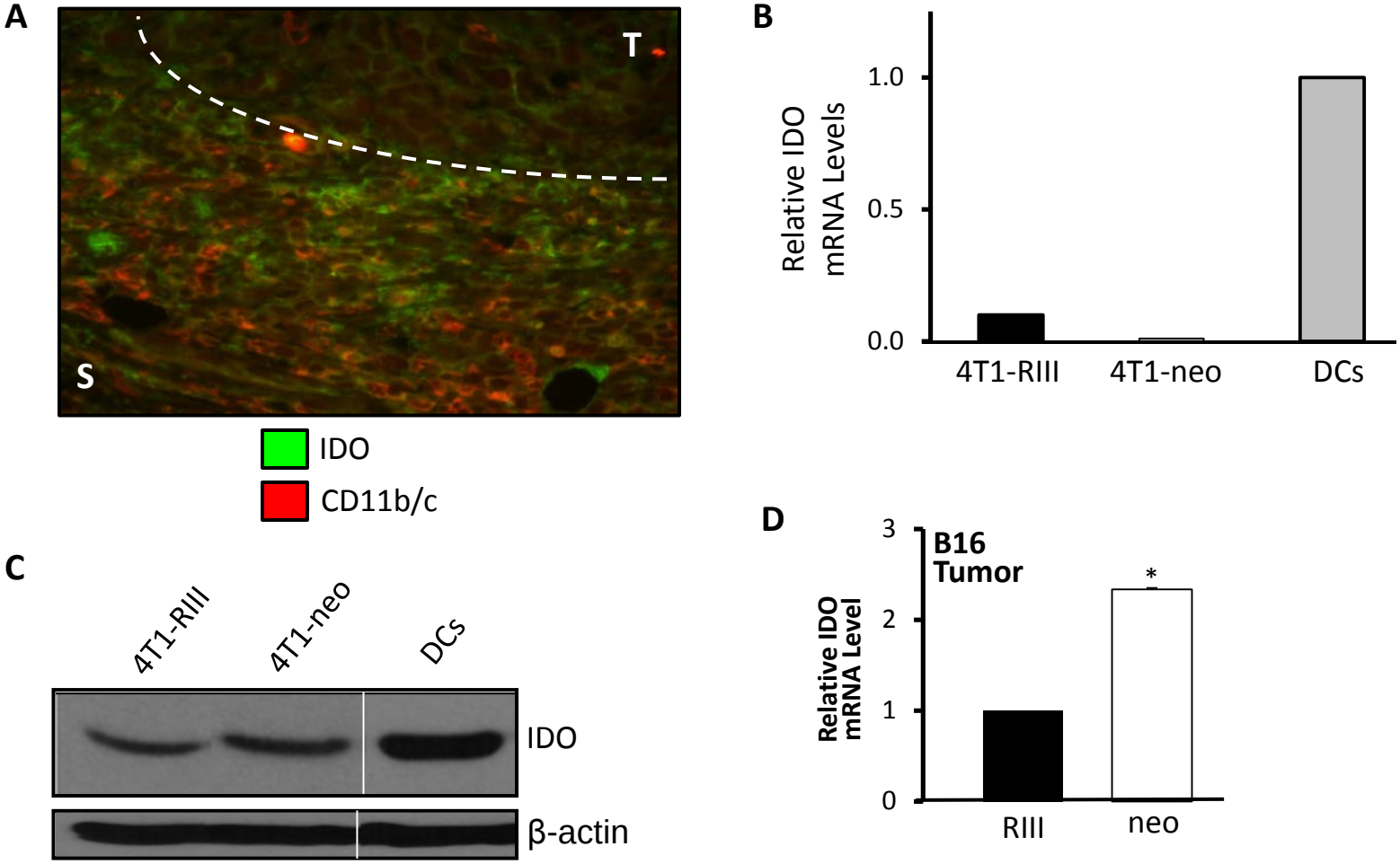

Supplementary Figure 12. IDO is Predominantly Expressed in the Stroma of 4T1 Tumors. (A) IDO immunofluorescence study of 4T1 tumors. IDO, green; CD11b/c, myeloid marker, red; T, tumor tissue; S, stromal tissue; dashed line, tumor-stroma border. Representative of 10 60x fields over two tumors. **(B)** IDO qRT-PCR in 4T1-neo and 4T1-RIII tumor cell lines relative to BMDCs. Representative of 2 independent experiments. **(C)** Western blot analysis of IDO expression in 4T1-neo and 4T1-RIII tumor cell lines relative to BMDCs. Bands were detected on the same blot and extraneous lanes were removed as indicated by line. Representative of 2 independent experiments. Lanes were run on the same gel but were noncontiguous. **(D)** IDO qRT-PCR in resected B16-mOVA-neo and B16-mOVA-RIII tumor tissues. Representative of 3 independent experiments.

Supplementary Figure 13

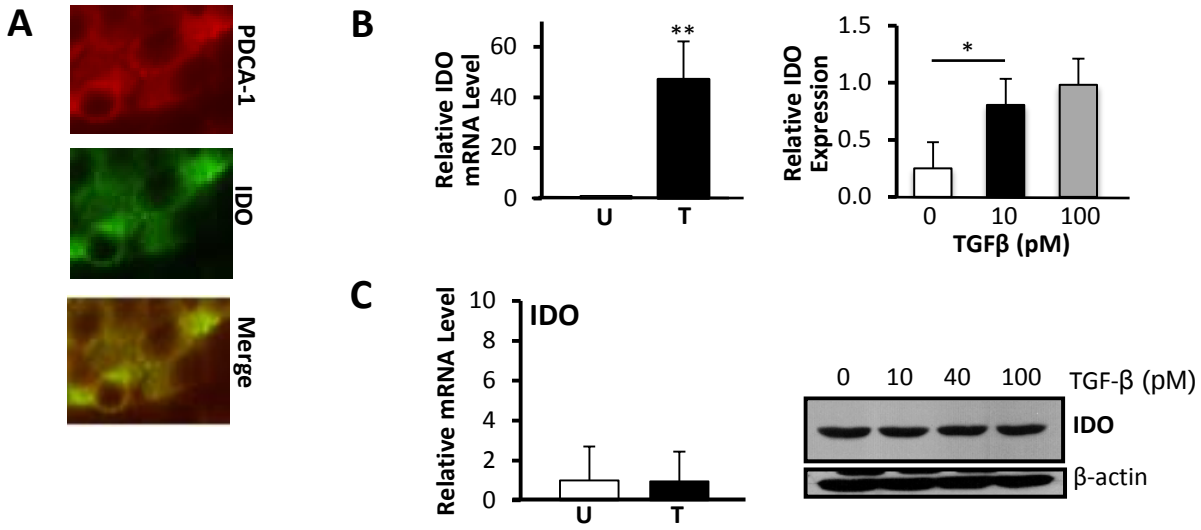

Supplementary Figure 13. Loss of TβRIII Induces the Upregulation of IDO by Local Plasmacytoid DCs. (A) pDC and IDO co-staining of TDLN tissues. 60x field. Representative of 3 TDLNs. **(B)** *left*, IDO qRT-PCR in TGF-β-treated splenic pDCs. U, untreated. T, TGF-β, 20 pM. *right,* IDO in-cell western of TGF-β-treated splenic pDCs. Performed in triplicate. Data representative of 2 independent experiments. **(C)** *left*, IDO qRT-PCR in TGF-β-treated BMDCs; *right*, Western blot analysis of IDO expression in BMDCs in the presence of increasing concentrations of TGF-β. All data is mean ± s.e.m. **P* < 0.05. Each is representative of 2 independent experiments.

Supplementary Figure 14

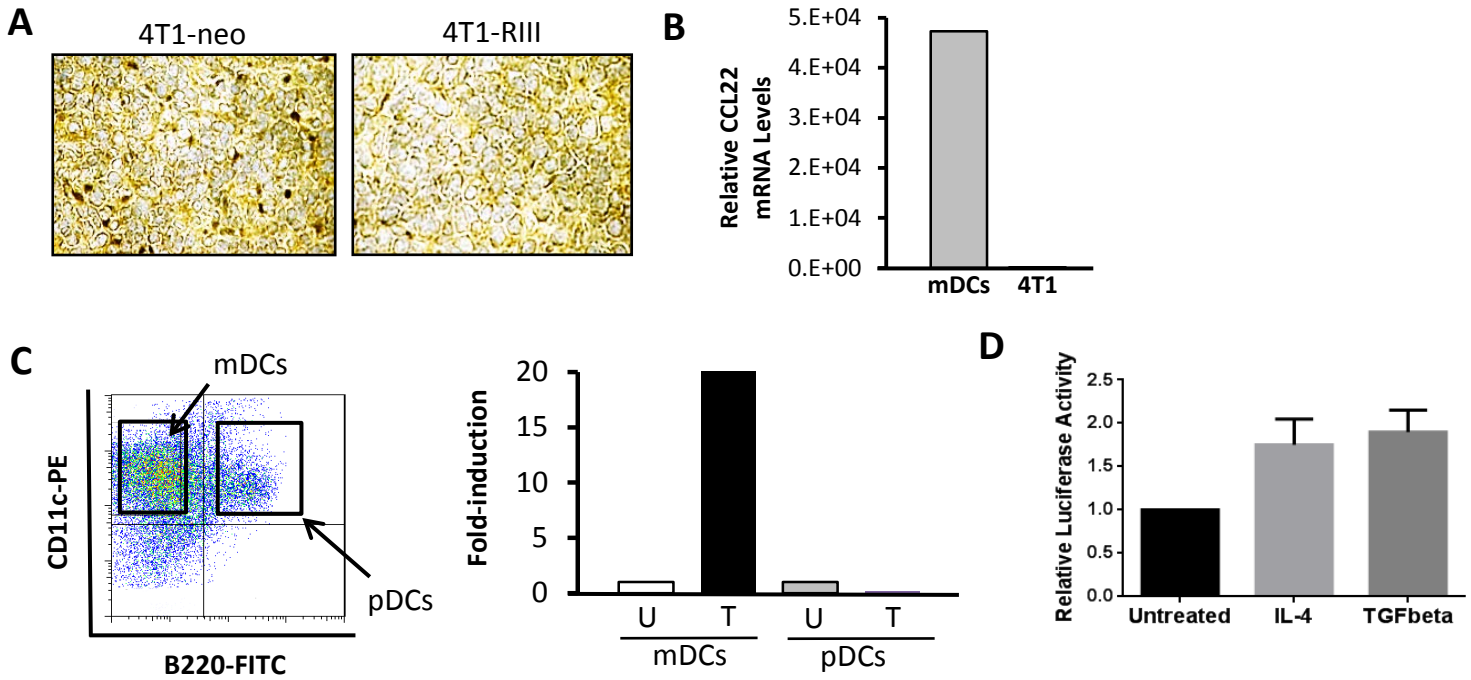

Supplementary Figure 14. TGF-β Stimulates CCL22 Expression by Myeloid DCs. (A) CCL22 IHC on resected 4T1-neo and 4T1-RIII primary tumors. Representative of 3 tumors examined per group. **(B)** Relative CCL22 qRT-PCR in 4T1 tumor cells and bone marrow-derived DCs. Experiment was repeated with the murine mammary carcinoma cell lines 167FARN, 4T07, 66CL4, and 4T1, all with similar results. **(C)** Murine bone marrow was expanded in the presence of Flt3L and sorted by FACS for mDC ($CD11c^{+}B220^{-}$) and pDC ($CD11c^{+}B220^{+}$) populations before incubating with TGF-β. RNA was isolated and CCL22 qRT-PCR analysis was performed. U, untreated, T, TGF-β. **(D)** COS7 cells were transfected with a CCL22 promoter-luciferase construct and treated with IL-4 and TGF-β before luminescence was quantitated. Performed in triplicate. IL-4, positive control.

Supplementary Figure 15

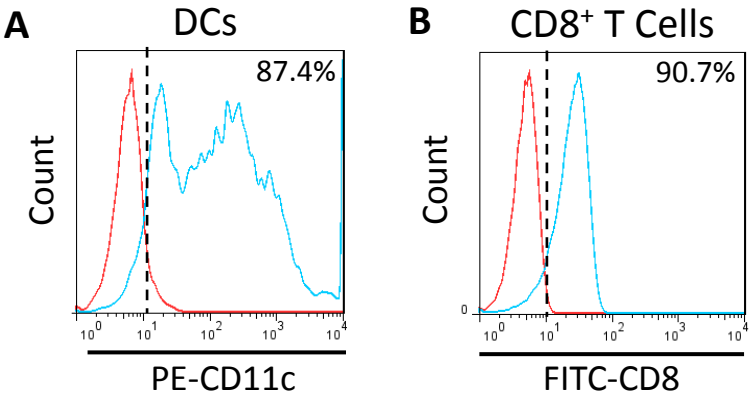

Supplementary Figure 15. Purification of Splenic DCs and CD8⁺ T cells from WT and CD11c^{dnRII} Transgenic Mice for TGF-β Signaling Studies. (A) Flow cytometry analysis of microbead-purified CD11c⁺ DCs (blue line). Isotype labeled unpurified splenocytes prior to magnetic column (red line). **(B)** Flow cytometry analysis of microbead purified CD8⁺ T cells (blue line). Isotype labeled unpurified splenocytes prior to magnetic column (red line).

Supplementary Figure 16

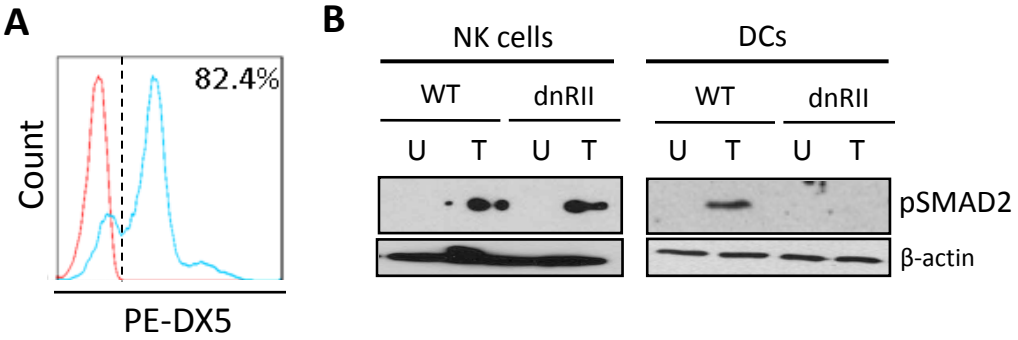

Supplementary Figure 16. NK Cells Isolated from CD11c^{dnRII} Transgenic Mice Exhibit an Intact TGF-β Signaling Axis. (A) Flow cytometry analysis of microbead-purified DX5^{+} NK cells (blue line). Isotype labeled unpurified splenocytes prior to magnetic column (red line). **(B)** pSMAD2 Western blot analysis of both NK cells and CD11c^{+} DCs isolated from the spleens of WT and CD11c^{dnRII} transgenic mice.

Supplementary Figure 17

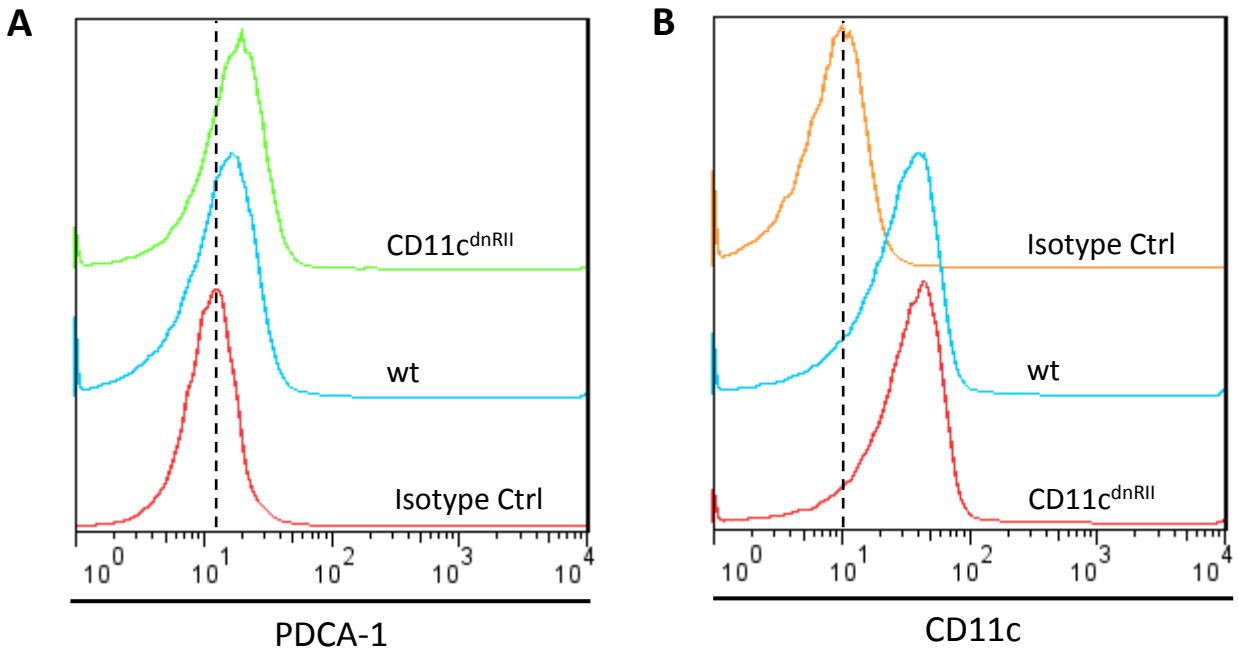

Supplementary Figure 17. DC Population Numbers Do Not Differ Significantly Between WT and CD11c^{dnRII} Transgenic Mice. (A) PDCA-1 flow cytometry analysis of resected WT and CD11c^{dnRII} lymph node tissues. **(B)** CD11c flow cytometry analysis of resected WT and CD11c^{dnRII} lymph node tissues. Lymph nodes harvested from two mice per group.

Supplementary Table 3

TβRIII, IDO, CCL22, and FoxP3 Expression by Normal Mammary Tissue and Invasive Breast Cancers.

Log2 median-centered ratio	TβRIII		IDO		CCL22		FoxP3	
	N	T	N	T	N	T	N	T
max	4.51	-0.82	2.69	4.134	2.73	2.95	1.66	2.05
90th	3.49	-0.82	0.78	2.788	1.56	2.22	0.82	0.91
75th	3.15	-0.82	0.17	1.411	0.90	1.66	0.55	0.63
median	2.69	-2.27	-0.64	0.459	0.51	1.08	0.17	0.44
25th	2.31	-2.35	-1.76	-1.11	-0.02	0.34	0.01	0.21
10th	1.98	-3.22	-2.37	-1.94	-0.36	0.06	-0.25	0.05
min	-1.38	-3.22	-3.08	-4.57	-1.26	-0.76	-0.64	-0.63

Data derived from the TCGA breast dataset, Oncomine 4.4. N, normal breast tissue. T, invasive breast cancer.

Supplementary Figure 18

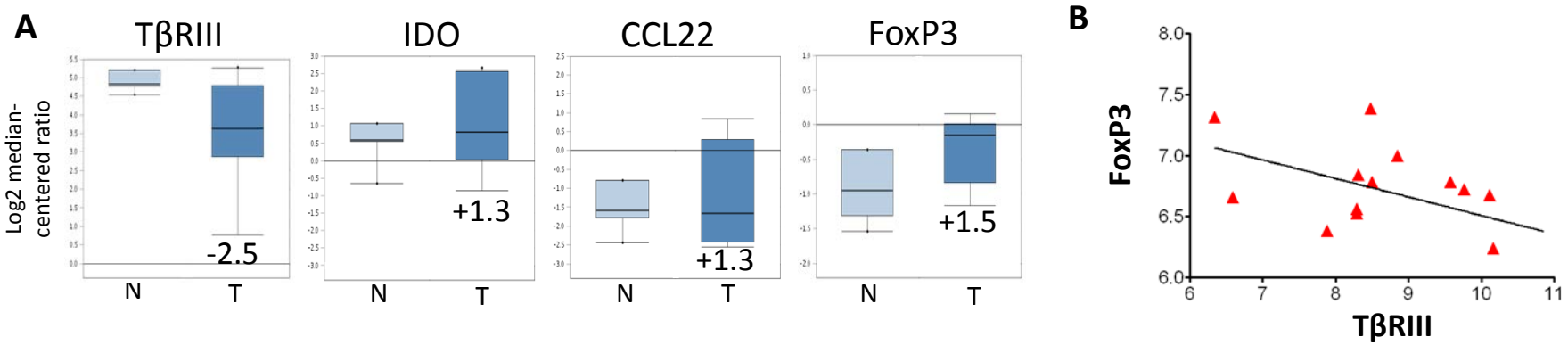

Supplementary Figure 18. ***In silico*** **IDO, CCL22, and FoxP3 Gene Expression Associations with TβRIII in Human Melanoma. (A)** Oncomine analysis of TβRIII, IDO, CCL22, and FoxP3 expression in human normal skin and melanoma tissues. See Supplementary Table 3. **(B)** Lower expression of TβRIII is associated with elevated FoxP3 expression levels in human melanoma tissues. *P* = 0.049.

Supplementary Table 4

TβRIII, IDO, CCL22, and FoxP3 Expression by Normal Skin Tissue and Primary Melanomas.

Log2 median-centered ratio	TβRIII		IDO		CCL22		FoxP3	
	N	T	N	T	N	T	N	T
max	5.21	5.27	1.06	2.65	-0.80	2.02	-0.36	0.54
90th	5.21	5.27	1.06	2.60	-0.80	0.84	-0.36	0.16
75th	5.21	4.78	1.06	2.56	-0.80	0.29	-0.36	0.01
median	4.83	3.64	0.60	0.82	-1.58	-1.66	-0.95	-0.16
25th	4.77	2.88	0.55	0.02	-1.78	-2.42	-1.32	-0.84
10th	4.59	0.76	-0.66	-0.85	-2.44	-2.56	-1.54	-1.17
min	4.54	0.67	-0.66	-2.55	-2.44	-2.83	-1.54	-1.43

Data derived from the Riker melanoma dataset, Oncomine 4.4. N, normal skin tissue. T, cutaneous melanoma.

Supplementary Figure 19

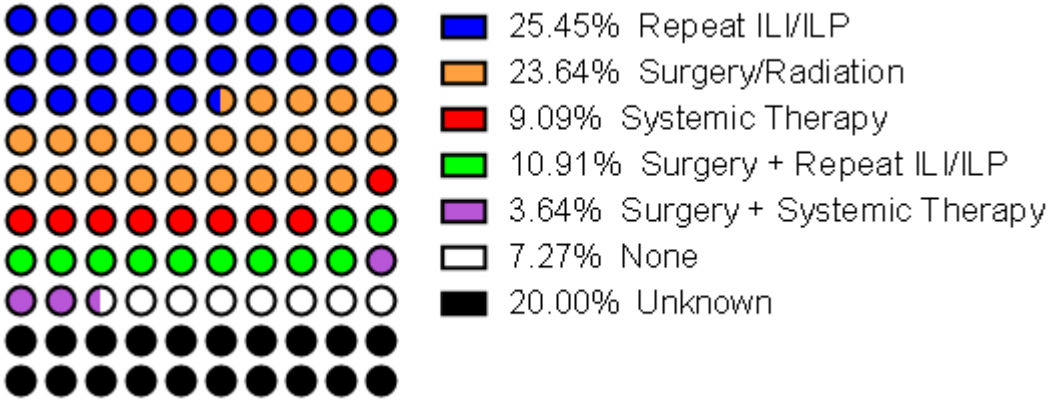

Supplementary Figure 19. Subsequent Therapies for Stage III Melanoma Patients Following Initial ILI. Overall response rates to ILI approximately 33%. ILP, isolated limb perfusion. Systemic therapy included temozolomide (1), DTIC (2), carboplatin/paclitaxel (1), sorafenib (1), bevacizumab (1), and interleukin-2 (1).

Supplementary Figure 20

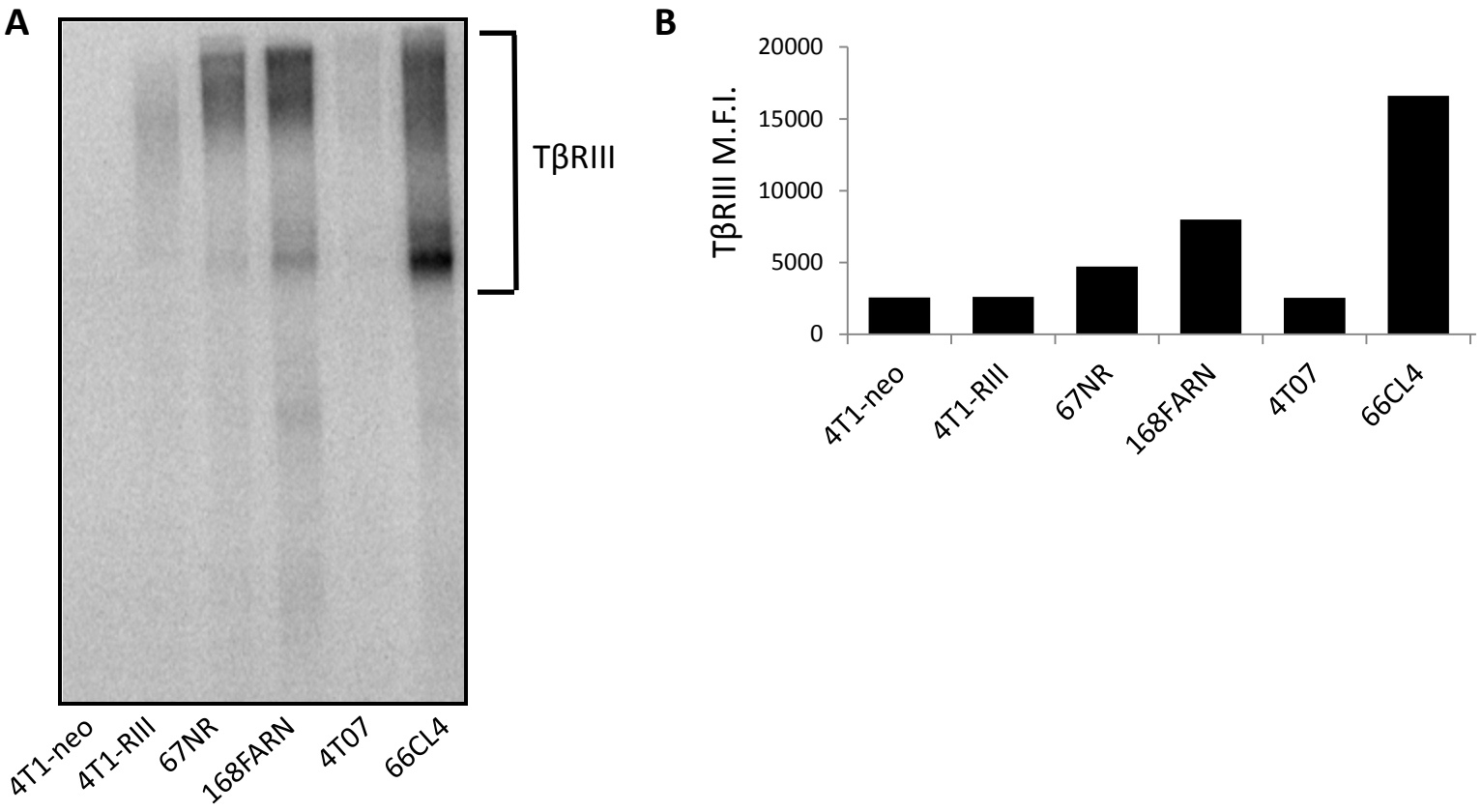

Supplementary Figure 20. The 4T1-RIII Stable Cell Line Exhibits Modest TβRIII Expression Relative to Other Murine Mammary Carcinoma Cell Lines. (A) ^{125}I-TGF-β binding and crosslinking study of TβRIII surface expression in the 4T1-RIII stable cell line relative to several other murine mammary carcinoma cell lines. **(B)** TβRIII surface expression by flow cytometry analysis correlates with binding and crosslinking results shown in **(A)**. M.F.I., mean fluorescence intensity.

Supplementary Table 5

Primer Name	Primer Sequence
mCD8-for	5’-CAGCAACTCGGTGATGTACT-3’
mCD8-rev	5’-TCCTCTGAAGGTCTGGGCTT-3’
mFoxP3-for	5’-TCCCACGCTCGGGTACAC-3’
mFoxP3-rev	5’-TTGCCAGCAGTGGGTAGGAT-3’
mIDO1-for	5’-CAGGCCAGAGCAGCATCTTC-3’
mIDO1-rev	5’-GCCAGCCTCGTGTTTTATTCC-3’
mCCL22-for	5’-GGTCCCTATGGTGCCAATG-3’
mCCL22-rev	5’-TTATCAAAACAACGCCAGGC-3’
mIL4-for	5’-TTGATGGGTCTCAACCCCCAGCT-3’
mIL4-rev	5’-CCGTGCATGGCGTCCCTTCTC-3’
mIL10-for	5’-GACCAGCTGGACAACATAC-3’
mIL10-rev	5’-CTGGAGTCCAGCAGACTC-3’
mIL13-for	5’-AGGCAGGCAGCAGCTTGAGC-3’
mIL13-rev	5’-GCTGCCGTGGCAGACAGGAG-3’
mIFNg-for	5’-TCAAGTGGCATAGATGTGGAA-3’
mIFNg-rev	5’-CACTCGGATGAGCTCATTGA-3’
CD11c-dnRII-for	5’-ACTTGACTGCACCGTTGTTGT-3’
CD11c-dnRII-rev	5’-ATGCCTTCTTCTCTTTCCTAC-3’

m, murine. for, forward primer. rev, reverse primer. dnRII, dominant-negative type II TGF-β receptor.